Sec-Eliminating the SARS-CoV-2 by AlGaN Based High Power Deep Ultraviolet Light Source

Shangfeng Liu, Wei Luo, Dan Li, Ye Yuan, Wei Tong, Junjie Kang, Yixin Wang, Duo Li, Xin Rong, Tao Wang, Zhaoying Chen, Yongde Li, Houjin Wang, Weiyun Wang, Jason Hoo, Long Yan, Shiping Guo, Bo Shen, Zhe Cong,* and Xinqiang Wang*

The world-wide spreading of coronavirus disease (COVID-19) has greatly shaken human society, thus effective and fast-speed methods of non-daily-life-disturbance sterilization have become extremely significant. In this work, by fully benefitting from high-quality AlN template (with threading dislocation density as low as ≈6×10^8 cm^{-2}) as well as outstanding deep ultraviolet (UVC-less than 280 nm) light-emitting diodes (LEDs) structure design and epitaxy optimization, high power UVC LEDs and ultra-high-power sterilization irradiation source are achieved. Moreover, for the first time, a result in which a fast and complete elimination of SARS-CoV-2 (the virus causes COVID-19) within only 1 s is achieved by the nearly whole industry-chain-covered product. These results advance the promising potential in UVC-LED disinfection particularly in the shadow of COVID-19.

1. Introduction

The worldwide explosion of coronavirus disease (COVID-19) infection has impacted the whole of human society, particularly striking the highly developed modern civilizations. Accompanied by the dramatic freezing of the global economy, the "Global Integration" which is constructed by international transportation is also hampered by the pandemic. Unfortunately, despite that the highly developed international transportation system provides plenty of contributions to human communication, it does inevitably do a great favor to virus dissemination. Therefore, an efficient, safe, and fast-speed germicidal program is in high demand. According to the character of disinfection, the popular avenues are mainly divided into two main series: i) chemical disinfectant like alcohol, chloride and strong oxidizer, etc., which easily breaks down the basic protein frame of viruses.[1–3] Although advanced by cost-efficiency and convenience, their anti-virus effect does not persist and in some cases is detrimental to human health; ii) to minimize the negative impact on social activities in public areas, physical treatment like ultraviolet (UV) light is preferable.[4] By fully employing the germicidal properties, the ultraviolet C (UVC) light (with wavelength of 180–280 nm) has been verified to destroy the chemical bonds inside the deoxyribonucleic acid (DNA) or ribonucleic acid (RNA) of microorganisms which is the genetic carrier for severe acute respiratory syndrome coronavirus 2 (SARS-CoV-2), the virus causing COVID-19.[5] The UVC light irradiation has been commonly used in hospital settings to disinfect objects which are impossible to immerse in liquid germicidal agents and to disinfect frequently-contacted surfaces.[6] According to the update from the International UV Association (IUVA), UVC light disinfection has been used extensively for more than 40 years, and it is reported that hundreds of bacteria and viruses tested to date, including two other coronaviruses (SARS-CoV-1 and MERS-CoV), and the UVC light presents an unambiguous contribution to sterilization. Moreover, it is particularly worth noting that the UVC light irradiation is helpful to prevent COVID-19 transmission by reducing contamination, thus unambiguously announcing the promising potential of UVC light irradiation source.[7] In these cases, the UVC light is mainly produced by a low-pressure mercury lamp, which is however made from the mercury that is ozone-toxic to human health.[8] Moreover, according to the Minamata Convention on Mercury signed in 2013, the manufacture, import, and export of a myriad of products containing mercury have been prohibited since 2020. Therefore, a safe and rapid germicidal candidate is eagerly sought.

As an alternative to mercury lamps, AlGaN based UVC-light-emitting diodes (LEDs) present much higher power density,

S. Liu, Dr. Y. Wang, D. Li, Dr. X. Rong, Dr. T. Wang, Dr. Z. Chen, Prof. B. Shen, Prof. X. Q. Wang
State Key Laboratory of Artificial Microstructure and Mesoscopic Physics
School of Physics, Nano-Optoelectronics Frontier Center of Ministry of Education (NFC-MOE)
Peking University
Beijing 100871, China
E-mail: wangshi@pku.edu.cn
Dr. W. Luo, Dr. Y. Yuan, Dr. J. Kang, Y. Li, H. Wang, W. Wang, Prof. X. Q. Wang
Songshan Lake Materials Laboratory
Dongguan, Guangdong 523808, China
D. Li, W. Tong, Prof. Z. Cong
Institute of Laboratory Animal Science (ILAS)
Chinese Academy of Medical Sciences
Beijing 100021, China
E-mail: congz@cnilas.org
Dr. J. Hoo, Dr. L. Yan, Dr. S. Guo
Advanced Micro-Fabrication Equipment Inc.
Shanghai 201201, China

therefore are naturally suitable (already applied in some cases, e. g. water purification, air, and surfaces anti-bacterial) for various disinfection purposes.[9–13] Although Nunayon et al. has confirmed the outstanding disinfection performance of UVC-LEDs in impeding/extirpating indoor bioaerosol of influenza viruses H_1N_1 and H_3N_2 (who are also coronaviruses), which is competitive with mercury lamps, the direct experimental evidence reported for eliminating the SARS-CoV-2 with UVC is very limited, especially, there is no report for the ultra-fast elimination.[14] In addition, despite numerous development efforts, UVC LEDs are still facing many challenges in the viewpoint of material issues, especially the growth of AlN films with low threading dislocation density (TDD).[10,11,15–19] Because of the lack of large size bulk AlN substrates, heteroepitaxial AlN films on foreign substrates such as sapphire are widely adopted.[20–22] It is well known that high-density TD caused by heteroepitaxy greatly affects the radiative property and reliability.[21,23–27] Besides, the strain in AlN films can affect the epitaxy growth and strain of the following AlGaN layer and active region, which directly influences the performance of UVC LEDs.[22,28] Therefore, high-quality crack-free AlN films are in great demand to realize high-efficiency AlGaN-based UVC LEDs, as well as the experimental evidence of their effective elimination of SARS-CoV-2.

In this work, an ultra-high power UVC irradiation source is fabricated and ultra-efficient sterilization treatment of UVC light particularly to SARS-CoV-2 is demonstrated for the first time. High quality AlN template with threading dislocation density as low as 6×10^8 cm^{-2} has been grown, which leads to the high performance of following UVC LEDs with a typical emission power of 10 mW at 100 mA for chip size of 10 mil × 20 mil. Those chips are then integrated into a UVC sterilization light source with a chip array of 15 × 13 at a size of 3.0 × 3.6 cm^2, with a typical emitting power as high as 2 W at a current of 1.3 A. That UVC light source is found to completely eliminate the SARS-CoV-2 virus with a concentration of 100 CCID$_{50}$/0.05 mL within only 1 s, showing the outstanding sterilization performance.

2. Results and Discussion

2.1. High Quality Epitaxial Growth of UVC LED Wafer and Characterization

As a crucial prerequisite to realize high-performance UVC LEDs, AlN templates with high crystal quality and low TDD (less than 1×10^9 cm^{-2}) are essential to realize a high enough internal quantum efficiency (IQE).[20] For this research, nano-patterned sapphire substrates (NPSSs) are used to prepare the AlN template by metal-organic chemical vapor deposition (MOCVD) with an epitaxial lateral overgrowth (ELOG) process. NPSSs are chosen as the substrate due to the fact that dislocations can be heavily annihilated at the crystal sidewalls. On the other hand, the pattern of NPSS scatters the output light from multiple quantum wells (MQWs) and thus can enhance the light extraction efficiency. It is worth noting that such an outstanding AlN/NSPP template does not merely contribute to the UVC-LED, but also is promising for other types of nitrides-based devices such as UV detectors and power devices.[29–34] Atomic force microscopy (AFM) image shown in **Figure 1**a
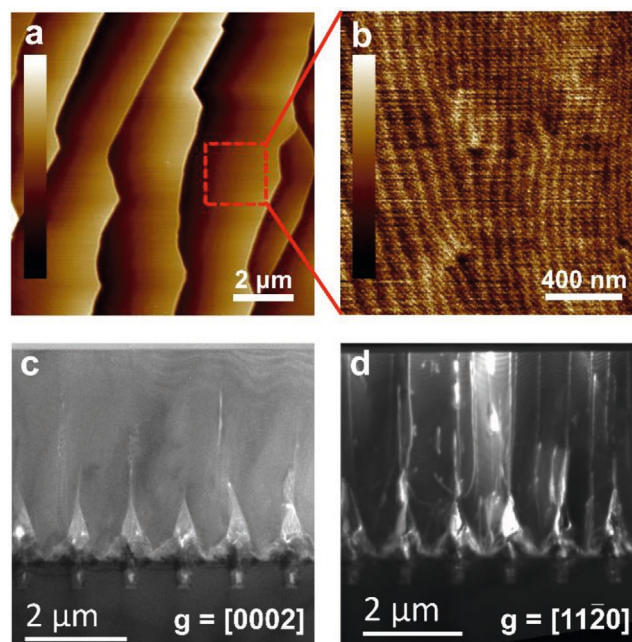

Figure 1. AFM image of the surface of AlN layer grown on NPSS substrate in a scanned area of a) 10 × 10 μm^2 (scale bar: 14 nm) and b) 2 × 2 μm^2 (scale bar: 0.6 nm) with an RMS roughness of about 0.09 nm. Cross-sectional dark-field STEM images under two-beam conditions for AlN grown on NPSS with c) g = [0002], and d) g = [11$\bar{2}$0]. Based on the standard Burgers vector analysis using invisibility criterion g · b = 0, the screw-type and edge-type dislocation lines are observed in (c) and (d), respectively.

reveals a typical step-bunching morphology of the smooth as-grown AlN surface on NPSS. Such step-bunching morphology is typically observed in AlN grown on both flat sapphire substrates and NPSSs, which is caused by the relatively high Al adatom diffusion length due to high growth temperature for AlN (usually above 1150 °C).[35] This kind of step-bunching morphology is in fact a trade-off for the following epitaxy of LED structure. On the one hand, the step-bunching leads to compositional inhomogeneity in the subsequently grown AlGaN layer, which negatively affects the efficiency of the UV LED devices.[36] On the other hand, the step-bunching redirects the pre-existing dislocation lines during the growth, and thus improving the crystal quality and device performance.[37,38] In this experiment, we modified the growth temperature and V/III ratio to control the surface morphology. And the step-bunching density is modulated to get a trade-off and the root mean square (RMS) roughness in a scanned area of 2 × 2 μm^2 is as low as 0.09 nm (as shown in Figure 1b). The crystallization of the AlN template is analyzed by cross-sectional transmission electron microscopy (TEM) measurement. Figures 1c,d show the cross-sectional dark-field STEM images of AlN epilayers on NPSS under two-beam conditions with g = [0002] and [11$\bar{2}$0], in which the screw-type and edge-type dislocations are placed into contrast. It is seen that few screw-type dislocations exist. Numerous edge-type dislocations are generated from the mesa, attributed to the merging of AlN grains. Most edge-type dislocations bend towards the sidewalls of interval voids by the driving of image force, hence residual threading dislocations mainly originate from the crystal grain merging in the pattern area.[39] The incoherent coalescing of misaligned crystal
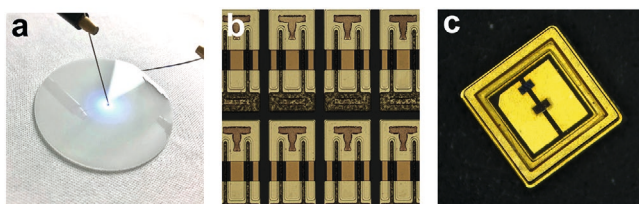
sidewalls (influenced by the hole diameter and the slope of growth fronts) would generate basal-plane dislocations with burger's vector $b = \frac{1}{3}\langle 11\bar{2}0 \rangle$, accompanied by the formation of low angle grain boundaries and stacking faults.[25,40,41] In our case, the coalescing speed and slope of growth fronts were controlled by adjusting growth temperature and V/III ratio to alleviate incoherent boundary related edge-dislocations. Calculated from the TEM measurement results, threading dislocation density is ≈6×10^8 cm^{-2}, which is qualified to improve the performance of UVC-LEDs. By the way, the crystal quality of the AlN template is also characterized by X-ray diffraction (XRD) and the FWHMs of XRD ω-rocking curves for (0002) and $(10\bar{1}2)$ plane are 134 and 236 arcsec, respectively. According to Mosaic model, the corresponding densities of the screw and edge-type dislocations are estimated to be 3.9×10^7 and 5.5×10^8 cm^{-2}, respectively, which are consistent with the estimated values from TEM measurement.[42]

Based on the above well-crystallized AlN template, UVC LED is grown by MOCVD, with a typical schematic structure shown in **Figure 2**a. By designing the composition in quantum well region and epitaxial process, UVC LED wafers with the emission wavelength of 275 nm are fabricated, by considering the trade-off between sterilization ability and wall-plug efficiency (WPE).[4] Figure 2b shows the XRD reciprocal space map (RSM) of $(10\bar{1}5)$ plane of the as-grown UVC LED wafer.

Since the in-plane lattice constant a is proportional to $1/Q_X$, it is shown that the n-Al$_{0.64}$Ga$_{0.36}$N layer is nearly coherently grown on the AlN template with a relaxation degree of only 4.2% which is much smaller than that of n-Al$_{0.60}$Ga$_{0.40}$N layer grown on the AlN template on flat sapphire (≈20%).[43] It has been verified that the strain relaxation of n-AlGaN is crucial to the IQE of emission from quantum wells by modulating the density of dislocations, furthermore contributing to the performance of LED, for example, in UVA and UVB device.[44,45] For various kinds of AlGaN-based LEDs with different Al compositions, a relatively low strain relaxation is preferred to achieve low TDDs. Herein, the low relaxation ratio of ≈4.2% promises a high quality of n-Al$_{0.64}$Ga$_{0.36}$N layer, which is the prerequisite to achieve the satisfied IQE as high as 60%. The FWHMs of XRD ω-rocking curves for (0002) and $(10\bar{1}2)$ plane of n-Al$_{0.64}$Ga$_{0.36}$N layer are 181 and 279 arcsec, respectively (with an estimated TDD is 7.2×10^8 cm^{-2}), showing high crystalline quality. The high-quality indicates that the low TDD of bottom AlN film is well maintained by suppressing the generation of interfacial misfit dislocation between AlN and AlGaN. By referring to the $(10\bar{1}5)$ RSM position of bulk AlN (marked with a black solid circle), it is found that the AlN/NPSS endorses tensile strain. The in-plane lattice constant a is calculated as 0.3125 nm from the equation $a = \lambda/(\sqrt{3}Q_X)$, where $\lambda = 0.15406$ nm is the wavelength of the X-ray and the Q_X is 0.2846 rlu derived from the $(10\bar{1}5)$ RSM. Thus the in-plane
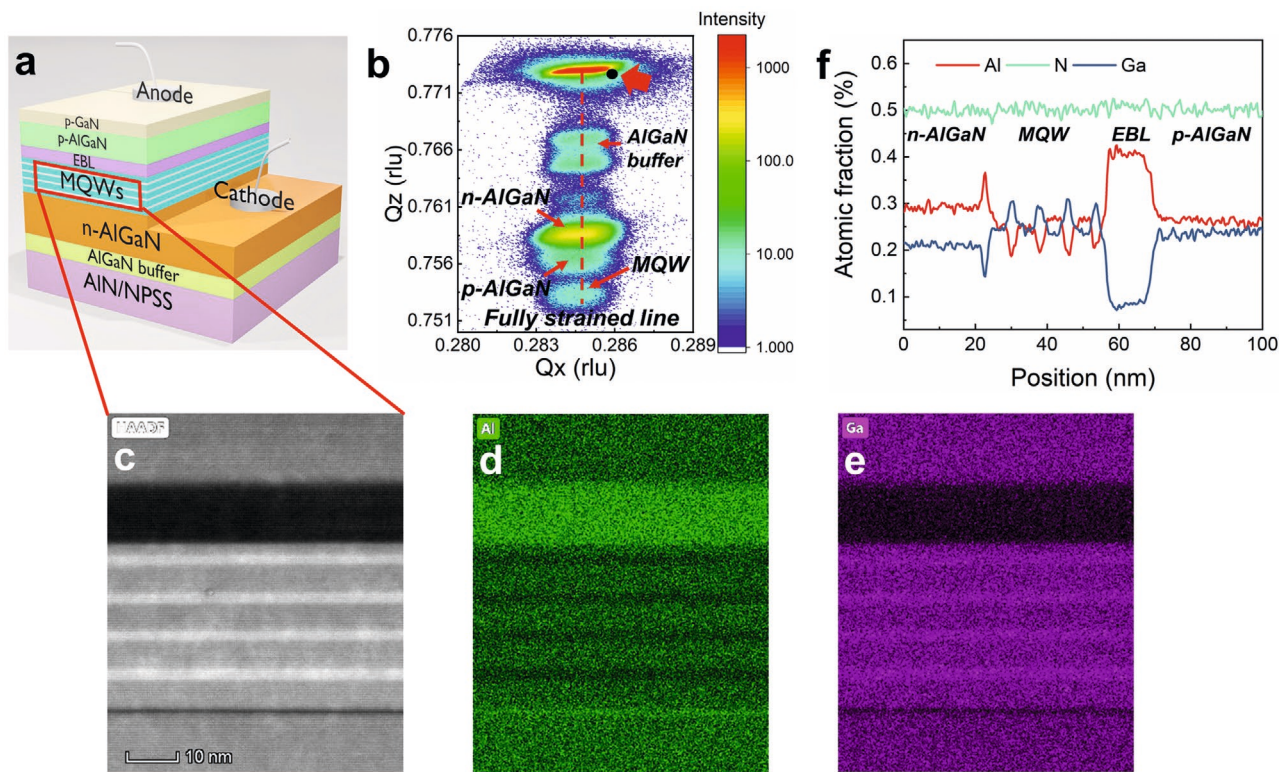
Figure 2. a) Schematic diagram of the UVC LED structure grown by MOCVD on AlN/NPSS template. b) XRD $(10\bar{1}5)$ RSM of the as-grown UVC LED wafer. The red dashed line presents the reciprocal space position which is fully strained to the AlN template (without relaxation). c) HAADF-STEM image of the MQWs in UVC LED, the corresponding EDS mapping of d) Al and e) Ga elements and f) the EDS line scan curve is also presented to give a quantitative description of the Al composition distribution. It shows 4 periods of MQW emitting region consisting of approximately 2 nm-thick Al$_{0.40}$Ga$_{0.60}$N wells and 5 nm-thick Al$_{0.52}$Ga$_{0.48}$N barrier layers.

**ADVANCED
SCIENCE NEWS**
www.advancedsciencenews.com

**ADVANCED
FUNCTIONAL
MATERIALS**
www.afm-journal.de

Figure 3. a) The electroluminescence demonstration of the as-grown UVC LED wafer. The visible blue-violet light originates from defect luminescence in the MQWs region since the UVC emission is not visible. b) The 10 × 20 mil square chips produced by UVC-LED wafer, and interdigitated finger electrode pattern is designed to adverse the current lateral spreading. c) Demonstration of UVC LED device adopting flip-chip packaging technology.

strain $\varepsilon_{//}$ ($\varepsilon_{//} = (a - a_{bulk\ AlN})/a_{bulk\ AlN}$, $a_{bulk\ AlN} = 0.3112$ nm) of AlN on NPSS is calculated to be 0.43%. It has been reported that, for AlN grown on hole-type NPSS, tensile stress is introduced into the AlN epilayer during the ELOG process caused by crystal coalescing.[46] The tensile strain of our AlN/NPSS provides a larger in-plane lattice constant which is closer to that of AlGaN, and thus leading to the nearly coherently grown n-AlGaN. Such a well crystallized n-AlGaN layer greatly benefits the growth of the MQWs. To confirm the high quality of MQWs, we performed high-angle annular dark-field scanning transmission electron microscopy (HAADF-STEM) measurements, with a result shown in Figure 2c. The sharp interface

between AlGaN barriers and AlGaN wells and good periodicity are both observed. The relative darker layer is grown as the hole blocking layer, which is designed to increase the internal quantum efficiency. The corresponding energy dispersive X-ray spectroscopy (EDS) mapping of Figure 2c is presented in Figures 2d,e, where the green and purple colors represent the Al and Ga elements, respectively. The EDS line-scan was performed across the MQW region in the growth direction to quantitatively confirm our design, as shown in Figure 2f. It is confirmed that the interfaces between the barrier and well layers in the MQWs are exactly abrupt, exhibiting negligible atom interdiffusion which guarantees the carrier recombination efficiency.

2.2. High Power Integrated UVC Light Source and SARS-CoV-2 Sterilization

The UVC LED wafers were then manufactured into chips with an area of 10 mil × 20 mil (**Figure 3**a,b). An interdigitated finger electrode array is designed to minimize the adverse effect of current lateral spreading on the efficiency, as shown in Figure 3b.[47] Because of the relatively narrow bandgap of p-type GaN, which enables the high absorption of the target UVC light (275 nm), a standard flip chip method was adopted during the packaging process to enhance the light extraction (Figure 3c). **Figure 4**a shows the current dependence of the output power of
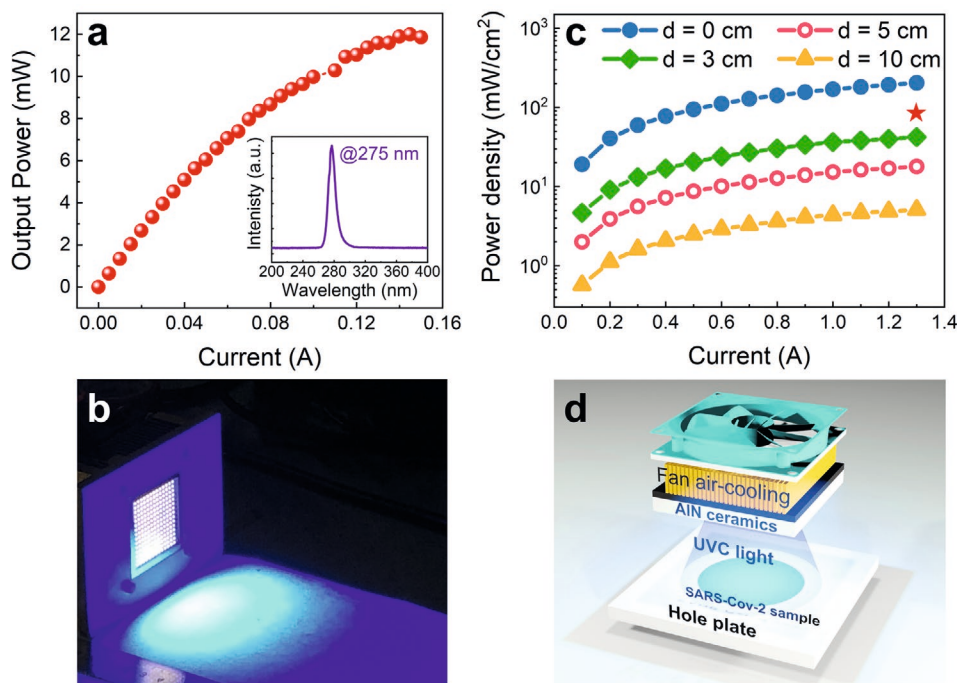
Figure 4. a) Output power versus current curve of a single packaged UVC LED (the electroluminescence spectrum is given in the inset). b) Demonstration of integrated sterilization light source fabricated by UVC-LEDs (without SARS-CoV-2 sample). This integrated array is composed of 13 parallel connected units and each unit includes 15 UVC LEDs in series connection. c) Current dependent power density at different distances from the irradiation source. The output power density obeys an inverse-square law as a dependence of irradiation distance, suggesting the importance of choosing a suitable working distance. Considering the working efficiency of every single LED, a working current of 1.3 A is chosen for the integrated source, in which condition each device works at 100 mA. The output power density adjacent to the array (d = 0) is 192 mW cm^{-2} at 1.3 A. The working point in the virus eliminating experiment is marked by a red star (94 mW cm^{-2}). d) The schematic image of the virus eliminating experiments.

a single packaged UVC LED. The output power amounts up to 10 mW at a working current of 100 mA. It is observed that the output power tends to slightly saturate at a current of around 140 mA, expressing the efficiency reduction due to the heat sink effect. Calculated from the result in Figure 4a, an external quantum efficiency (EQE) of 2.65% at a forward current of 20 mA is obtained. The IQE is estimated to be about 60% by comparison between the integrated PL intensity of LEDs at 300 K and 10 K, respectively. In order to achieve high IQE and EQE, several methods have been proposed, such as optimizing the last barrier thickness in the MQW area, employing a transparent p-AlGaN contact layer, involving Rh mirror electrode and so on.[48,49] The electroluminescence spectrum is given in the inset, which shows an emission peak at 275 nm with an FWHM of ≈12 nm.

Subsequently, to obtain a high output power density, the UVC LED chips are integrated into an array of 15×13, with a whole area of 3.0×3.6 cm^2, as shown in Figure 4b. To solve the heat-accumulation in the case of high-power irradiation, the LED array is integrated on thermo-conductive AlN ceramics equipped with a fan air-cooling system. The working state of the integrated UVC light source is shown in Figure 4b. To estimate the irradiation performance of the integrated UVC light source, the output power densities at different distances to the array surface are measured, as shown in Figure 4c. One has to note that despite output power density is in inverse proportion to the square of irradiation distance, an exposure distance within several centimeters still fulfills plenty of sterilization demands, particularly in the cases in which a high sterilization-speed is preferred, for example, flowing water and flowing air in air conditioning pipe.

To examine the sterilization treatment of our integrated UVC light source to SARS-CoV-2, an infection experiment was carried out in Institute of Laboratory Animal Science, Chinese Academy of Medical Sciences, as described in detail below: The experimental samples with SARS-CoV-2 (the virus titer of the solution is 100 CCID$_{50}$/0.05 mL) were treated with UVC light source with an exposure time of 1 s, as shown in Figure 4d. A virus control group without UVC treatment was also set up as a reference. Then two groups of solutions were diluted into 4 series with various concentrations of 100, 10, 1, and 0.1 CCID$_{50}$/0.05 mL, and were subsequently added to solutions with Vero cells. Afterward, all samples were cultivated together with a Vero cell control group without virus for 5 days. According to the cytopathic observation (**Table 1**), it is concluded that the treatment with an exposure time of 1 s enables 100% elimination of the SARS-CoV-2 at the cellular level. Particularly, such a short eliminating period is highly admired due to its negligible disturbance to people's daily lives. For the commonly used ethanol and 2-propanol sterilization solution at a concentration above 30% (vol/vol), with whom a continuous treatment with a period of 30 s is possible to inactivate coronavirus.[50] As presented in Table 1, when placing unirradiated samples as references, the one-second UVC-treated specimens whose original virus concentration is 0.1, 1, and 10, as well as 100 CCID$_{50}$/0.05 mL, respectively, all show zero positive rates, unambiguously consolidating the remarkable sterilization of UVC-LED to SARS-CoV-2.

Table 1. The cytopathic observation results of the UVC irradiated group with an exposure time of 1 s, and the virus control group (without UVC irradiation) and cell control group (without virus) are placed for convenient comparison. The zero-positive rate of the irradiated group indicates a 100% elimination on the SARS-CoV-2 at the cellular level.

Exposure time [s]	Virus original concentration (CCID$_{50}$/0.05 mL)	Positive rate (%)	Calculated concentration (CCID$_{50}$/0.05 mL)
1	0.1	0	0
	1	0	
	10	0	
	100	0	
	0.1	0	100
0	1	50	
(Virus control group)	10	100	
	100	100	
Cell control group	–	–	–

"–" for cells with no CPE changes or normal cell morphology.

3. Conclusion

In summary, an efficient and ultra-fast sterilization treatment to SARS-CoV-2 is demonstrated for the first time using our ultra-high-power UVC irradiation source with the output power as high as 2 W at a current of 1.3 A. According to the sterilization experiment, an exposure time as short as one second is sufficient to realize a complete elimination of SARS-CoV-2. This extremely fast virus elimination by the high-power deep UV light highlights an avenue to solve the dilemma of weighing daily-life concerns and sterilization consequences, accelerating the adoption of UVC LEDs for application in the mitigation of the pandemic.

4. Experimental Section

Growth and Device Fabrication: The AlN films on NPSS and UVC LED structures were epitaxially grown in Prismo HiT3 MOCVD system. H$_2$ and N$_2$ were used as the carrier gas for the epitaxial process. Trimethyl-aluminum (TMAl), Trimethyl-gallium (TMGa), and ammonia (NH$_3$) were used as Al, Ga, and N precursors, respectively. Prior to the epitaxy of AlN films, a 15-nm-thick AlN layer was deposited on NPSS by magnetron sputtering as a nucleation layer. The AlN growth on NPSS is consisted of three steps: i) a 200-nm-thick layer growth in 3D mode (temperature = 1100 °C, pressure = 100 Torr); ii) the lateral overgrowth with a thickness of 1.8 µm (temperature = 1250 °C, pressure = 40 Torr); iii) a 2-µm continuing growth (temperature = 1200 °C, pressure = 30 Torr). Those AlN layers are then used as templates for following growth. A 200 nm thick homoepitaxial AlN buffer layer was typically grown first, followed by the UVC LED structure. After epitaxial growth, the standard UVC LED chip processing was carried out by mask layer deposition, photolithography, reactive ion etching, and sputtering techniques to make 10×20 mil square chips.

Characterization: XRD measurement was performed by PANalytical X'Pert3 MRD XL system using Cu Kα_1 X-ray source. Surface morphology was measured by AFM in tapping mode. The HAADF-STEM was carried out in a Thermo fisher FEI Themis Z Cs probe-corrected STEM system operated at 200kV.

Supporting Information

Acknowledgements

Conflict of Interest

The authors declare no conflict of interest.

Keywords

[1] N. Ogata, M. Sakasegawa, T. Miura, T. Shibata, Y. Takigawa, K. Taura, K. Taguchi, K. Matsubara, K. Nakahara, D. Kato, K. Sogawa, H. Oka, *Pharmacology* **2016**, *97*, 301.

[2] R. Abbasi, R. Jain, K. Nelson, D. Busche, D. M. Lynn, N. L. Abbott, *Adv. Funct. Mater.* **2019**, *29*, 1804851.

[3] E. Ruiz-Hitzky, M. Darder, B. Wicklein, C. Ruiz-Garcia, R. Martín-Sampedro, G. del Real, P. Aranda, *Adv. Healthcare Mater.* **2020**, *9*, 2000979.

[4] M. Buonanno, D. Welch, I. Shuryak, D. J. Brenner, *Sci. Rep.* **2020**, *10*, 10285.

[5] F. J. Garcia de Abajo, R. J. Hernandez, I. Kaminer, A. Meyerhans, J. Rosell-Llompart, T. Sanchez-Elsner, *ACS Nano* **2020**, *14*, 7704.

[6] B. Casini, B. Tuvo, M. L. Cristina, A. M. Spagnolo, M. Totaro, A. Baggiani, G. P. Privitera, *Int. J. Environ. Res. Public Health* **2019**, *16*, 3572.

[7] IUVA Fact Sheet on UV Disinfection for COVID-19, https://iuva.org/IUVA-Fact-Sheet-on-UV-Disinfection-for-COVID-19 (accessed: October 2020).

[8] J. F. da Silveira Petruci, P. R. Fortes, V. Kokoric, A. Wilk, I. M. Raimundo, A. A. Cardoso, B. Mizaikoff, *Sci. Rep.* **2013**, *3*, 3174.

[9] Y. H. Ra, S. Kang, C. R. Lee, *Adv. Opt. Mater.* **2018**, *6*, 1701391.

[10] Y. Wang, X. Rong, S. Ivanov, V. Jmerik, Z. Chen, H. Wang, T. Wang, P. Wang, P. Jin, Y. Chen, V. Kozlovsky, D. Sviridov, M. Zverev, E. Zhdanova, N. Gamov, V. Studenov, H. Miyake, H. Li, S. Guo, X. Yang, F. Xu, T. Yu, Z. Qin, W. Ge, B. Shen, X. Wang, *Adv. Opt. Mater.* **2019**, *7*, 1801763.

[11] D. Li, K. Jiang, X. Sun, C. Guo, *Adv. Opt. Photonics* **2018**, *10*, 43.

[12] W. Luo, B. Liu, Z. Li, L. Li, Q. Yang, L. Pan, C. Li, D. Zhang, X. Dong, D. Peng, F. Yang, R. Zhang, *Appl. Phys. Lett.* **2018**, *113*, 072107.

[13] J. Dai, B. Liu, Z. Zhuang, G. He, T. Zhi, T. Tao, Q. Xu, Y. Li, H. Ge, Z. Xie, R. Zhang, *Nanotechnology* **2017**, *28*, 385205.

[14] W. Szeto, W. C. Yam, H. Huang, D. Y. C. Leung, *BMC Infect. Dis.* **2020**, *20*, 127.

[15] Z. Chen, Z. Liu, T. Wei, S. Yang, Z. Dou, Y. Wang, H. Ci, H. Chang, Y. Qi, J. Yan, J. Wang, Y. Zhang, P. Gao, J. Li, Z. Liu, *Adv. Mater.* **2019**, *31*, 1807345.

[16] X. Rong, X. Wang, S. V. Ivanov, X. Jiang, G. Chen, P. Wang, W. Wang, C. He, T. Wang, T. Schulz, M. Albrecht, V. N. Jmerik, A. A. Toropov, V. V. Ratnikov, V. I. Kozlovsky, V. P. Martovitsky, P. Jin, F. Xu, X. Yang, Z. Qin, W. Ge, J. Shi, B. Shen, *Adv. Mater.* **2016**, *28*, 7978.

[17] F. Li, L. Wang, W. Yao, Y. Meng, S. Yang, Z. Wang, *Superlattices Microstruct.* **2020**, *137*, 106336.

[18] K. Uesugi, Y. Hayashi, K. Shojiki, H. Miyake, *Appl. Phys. Express* **2019**, *12*, 6.

[19] B. H. Le, S. Zhao, X. Liu, S. Y. Woo, G. A. Botton, Z. Mi, *Adv. Mater.* **2016**, *28*, 8446.

[20] M. Kneissl, T.-Y. Seong, J. Han, H. Amano, *Nat. Photonics* **2019**, *13*, 233.

[21] R. G. Banal, M. Funato, Y. Kawakami, *Appl. Phys. Lett.* **2008**, *92*, 241905.

[22] M. Shatalov, R. Jain, T. Saxena, A. Dobrinsky, M. Shur, in *III-Nitride Semiconductor Optoelectronics*, Vol. *96*, (Eds: Z. Mi, C. Jagadish), Elsevier, Cambridge **2017**, Ch. 2.

[23] S.-i. Inoue, N. Tamari, M. Taniguchi, *Appl. Phys. Lett.* **2017**, *110*, 141106.

[24] T. Y. Wang, C. T. Tasi, C. F. Lin, D. S. Wuu, *Sci. Rep.* **2017**, *7*, 14422.

[25] L. Zhang, F. Xu, J. Wang, C. He, W. Guo, M. Wang, B. Sheng, L. Lu, Z. Qin, X. Wang, B. Shen, *Sci. Rep.* **2016**, *6*, 35934.

[26] B. T. Tran, N. Maeda, M. Jo, D. Inoue, T. Kikitsu, H. Hirayama, *Sci. Rep.* **2016**, *6*, 35681.

[27] H. Kobayashi, S. Ichikawa, M. Funato, Y. Kawakami, *Adv. Opt. Mater.* **2019**, *7*, 1900860.

[28] C. He, Z. Qin, F. Xu, L. Zhang, J. Wang, M. Hou, S. Zhang, X. Wang, W. Ge, B. Shen, *Appl. Phys. Express* **2016**, *9*, 051001.

[29] J. Li, Z. Fan, R. Dahal, M. Nakarmi, J. Lin, H. Jiang, *Appl. Phys. Lett.* **2006**, *89*, 213510.

[30] T. Wunderer, C. L. Chua, Z. Yang, J. E. Northrup, N. M. Johnson, G. A. Garrett, H. Shen, M. Wraback, *Appl. Phys. Express* **2011**, *4*, 092101.

[31] E. Cicek, R. McClintock, C. Cho, B. Rahnema, M. Razeghi, *Appl. Phys. Lett.* **2013**, *103*, 181113.

[32] Z. Lochner, T.-T. Kao, Y.-S. Liu, X.-H. Li, M. M. Satter, S.-C. Shen, P. D. Yoder, J.-H. Ryou, R. D. Dupuis, Y. Wei, H. Xie, A. Fischer, F. A. Ponce, *Appl. Phys. Lett.* **2013**, *102*, 101110.

[33] Z. Bryan, I. Bryan, S. Mita, J. Tweedie, Z. Sitar, R. Collazo, *Appl. Phys. Lett.* **2015**, *106*, 232101.

[34] R. Kirste, Q. Guo, J. H. Dycus, A. Franke, S. Mita, B. Sarkar, P. Reddy, J. M. LeBeau, R. Collazo, Z. Sitar, *Appl. Phys. Express* **2018**, *11*, 082101.

[35] A. Yoshikawa, T. Nagatomi, T. Morishita, M. Iwaya, T. Takeuchi, S. Kamiyama, I. Akasaki, *Appl. Phys. Lett.* **2017**, *111*, 191103.

[36] K. Jiang, X. Sun, J. Ben, Z. Shi, Y. Jia, Y. Wu, C. Kai, Y. Wang, D. Li, *CrystEngComm* **2019**, *21*, 4864.

[37] J. Bai, M. Dudley, W. H. Sun, H. M. Wang, M. A. Khan, *Appl. Phys. Lett.* **2006**, *88*, 051903.

[38] C. He, W. Zhao, H. Wu, S. Zhang, K. Zhang, L. He, N. Liu, Z. Chen, B. Shen, *Cryst. Growth Des.* **2018**, *18*, 6816.

[39] F. J. Xu, L. S. Zhang, N. Xie, M. X. Wang, Y. H. Sun, B. Y. Liu, W. K. Ge, X. Q. Wang, B. Shen, *CrystEngComm* **2019**, *21*, 2490.

[40] R. Jain, W. Sun, J. Yang, M. Shatalov, X. Hu, A. Sattu, A. Lunev, J. Deng, I. Shturm, Y. Bilenko, R. Gaska, M. S. Shur, *Appl. Phys. Lett.* **2008**, *93*, 051113.

[41] A. Kazaryan, Y. Wang, S. A. Dregia, B. R. Patton, *Phys. Rev. B* **2001**, *63*, 184102.

[42] M. A. Moram, M. E. Vickers, *Rep. Prog. Phys.* **2009**, *72*, 036502.

[43] M. A. Khan, N. Maeda, M. Jo, Y. Akamatsu, R. Tanabe, Y. Yamada, H. Hirayama, *J. Mater. Chem. C* **2019**, *7*, 143.

[44] M. A. Khan, Y. Itokazu, N. Maeda, M. Jo, Y. Yamada, H. Hirayama, *ACS Appl Electron Mater* **2020**, *2*, 1892.

[45] H. Murotani, H. Miyoshi, R. Takeda, H. Nakao, M. A. Khan, N. Maeda, M. Jo, H. Hirayama, Y. Yamada, *J. Appl. Phys.* **2020**, *128*, 105704.

[46] T.-Y. Wang, C.-T. Tasi, K.-Y. Lin, S.-L. Ou, R.-H. Horng, D.-S. Wuu, *Appl. Surf. Sci.* **2018**, *455*, 1123.

[47] H.-Y. Ryu, J.-I. Shim, *Opt. Express* **2011**, *19*, 2886.

[48] T. Takano, T. Mino, J. Sakai, N. Noguchi, K. Tsubaki, H. Hirayama, *Appl. Phys. Express* **2017**, *10*, 031002.

[49] M. A. Khan, E. Matsuura, Y. Kashima, H. Hirayama, *Phys. Status Solidi A* **2019**, *216*, 1900185.

[50] A. Kratzel, D. Todt, P. V'Kovski, S. Steiner, M. Gultom, T. T. N. Thao, N. Ebert, M. Holwerda, J. Steinmann, D. Niemeyer, R. Dijkman, G. Kampf, C. Drosten, E. Steinmann, V. Thiel, S. Pfaender, *Emerging Infect. Dis.* **2020**, *26*, 1592.